Sustainable Chemistry and Pharmacy 36 (2023) 101290

Contents lists available at ScienceDirect

Sustainable Chemistry and Pharmacy

journal homepage: www.elsevier.com/locate/scp

Facile synthesis of multi-stimuli responsive biocompatible trimethyl chitosan-based nanogel as potential nanocarrier for photothermal chemotherapy

Kritsadayut Lekjinda [a], Panya Sunintaboon [a, *], Phissinee Jakaew [b], Tuksin Jearanaiwitayakul [c], Sukathida Ubol [b], Ratchapol Jenjob [d, e], Sugeun Yang [d, e]

[a] Department of Chemistry, Faculty of Science, Mahidol University, Bangkok, Thailand
[b] Department of Microbiology, Faculty of Science, Mahidol University, Bangkok, Thailand
[c] Department of Clinical Pathology, Faculty of Medicine Vajira Hospital, Navamindradhiraj University, Bangkok, Thailand
[d] Department of Biomedical Science, BK21 FOUR Program in Biomedical Science and Engineering, Inha University College of Medicine, Incheon, South Korea
[e] Inha Institute of Aerospace Medicine, Inha University College of Medicine, Incheon, South Korea

ARTICLE INFO

Handling Editor: Fabio Aricò

Keywords:
Trimethyl chitosan
UCST-Type nanogel
Stimuli-responsive
Phototherapy
Chemotherapy

ABSTRACT

Development of multi-stimuli responsive nanocarriers for cancer treatment with combined or synergistic functionalities is highly attractive and challenging for overcoming the limitations related to single-stimuli responsive ones. Herein, we report the synthesis of multi-stimuli responsive biocompatible nanogel comprising crosslinked poly(2-hydroxyethyl methacrylate) core and trimethyl chitosan (TMC) periphery by a facile visible light-initiated surfactant-free emulsion polymerization, and its use as multi-stimuli responsive nanocarrier. Some of polymerization parameters, such as TMC type and crosslinker concentration were optimized, which were found to strongly affect the nanogel's thermoresponsiveness. At the optimal condition, using TMC (45% degree of quaternization) and 5% MBA crosslinker, the synthesized nanogel exhibited a reversible upper critical solution temperature (UCST)-type volume phase transition above 30 °C in acidic aqueous environment (pH 4.5–5). Moreover, the incorporation of sodium copper chlorophyllin as a bio-based photosensitive agent and honokiol model drug to such nanogel not only introduced the hyperthermic effect under light irradiation, but also triggered the release of encapsulated honokiol. The co-loaded nanogel, possessing combined photothermal and chemotherapeutic effect, enhanced the antitumor efficacy against Calu-3 cells. These results showed that the nanogel with pH- and light-dependent UCST-type thermoresponsiveness can be synthesized through the facile method and is promising for being used as multifunctional nanocarrier in cancer therapy.

1. Introduction

Dual- or multi-stimuli responsive nanogels are crosslinked polymeric particles having size ranging from 1 to 1000 nm (Qureshi and Khatoon, 2019), which can undergo structural changes (e.g., swelling or collapse) in response to a combination of two or more stimuli. Dual responsive systems based on temperature and light stimuli are often investigated for developing smart nanogels, as well

* Corresponding author.
E-mail address: panya.sun@mahidol.ac.th (P. Sunintaboon).

https://doi.org/10.1016/j.scp.2023.101290
Received 11 July 2023; Received in revised form 19 September 2023; Accepted 29 September 2023
Available online 14 October 2023
2352-5541/© 2023 Elsevier B.V. All rights reserved.

as microgels (Augé et al., 2020; Hu et al., 2021; Lee et al., 2019). Such nanogels can exhibit volume phase transitions and changes in polymer network structures by external stimuli, and have been applied for controlled release applications. Normally found in dual responsive nanogels, photothermal/photosensitive agents can be incorporated into thermoresponsive nanogels. These agents help transform the absorbed light energy (e.g., visible, NIR) into local heat, so-called hyperthermic effect (Chang and Tsai, 2018). The generated heat could not only directly kill the cancer cells, but also concurrently undergo thermal activation and triggering the release of encapsulated drug. One example of photothermal agents is sodium copper chlorophyllin (SCC), a porphyrin-containing molecule derived from natural chlorophyll, which provides low cytotoxicity, biodegradable properties and high efficiency for photothermal and photodynamic therapy (Chang et al., 2018; Chang and Tsai, 2018).

There have been a few reports in the literature concerning light- and temperature-responsive nanogels based on polymers with the upper critical solution temperature (UCST) behavior (Augé et al., 2020). Typically, UCST-type polymeric nanogels can undergo swelling upon heating due to the disruption of either reversible hydrogen bonding or electrostatic interaction among polymer chains at temperatures above the polymer's UCST (Jia et al., 2017). Over the past decade, significant progress has been made in developing polymers with UCST transitions close to physiological temperatures (Jia et al., 2017; Tong et al., 2016; Xu and Liu, 2018; Zhu et al., 2014, 2020).

Poly(2-hydroxyethyl methacrylate) (PHEMA) is a biocompatible thermoresponsive polymer with the UCST above 100 °C (Seuring and Agarwal, 2013). PHEMA contains hydrophilic repeating units, which cannot be dissolved in water due to the intra- and intermolecular hydrogen bonding between its hydroxyl side groups. However, the UCST of PHEMA could be adjusted to fall below 100 °C through copolymerization with cationic comonomers (Longenecker et al., 2011). The cationic moieties can help accelerate the breakage of hydrogen bonding upon heating and decrease its UCST to below 100 °C. For example, Longenecker et al. prepared PHEMA homopolymer and copolymers with different side chains, such as carboxylic acid, tertiary amine, and quaternary amine (Longenecker et al., 2011). They found that the resulting copolymers polymerized with comonomers containing only quaternary amine and protonated tertiary amine exhibited the UCST transition at approximately 80 °C. However, there are no reports of PHEMA's UCST behavior close to physiological conditions.

N,N,N-Trimethyl chitosan (TMC) is a partially quaternized chitosan derivative, bearing quaternary amine groups. It can be more readily soluble in aqueous media with a broader pH range than its underivatized counterpart, and also contain pH-responsive residues (e.g., 1°, 2°, 3° amines) *via* protonation/deprotonation (Ristić et al., 2015). The net positive charge of TMC in acidic media arises from both the permanently charged cationic quaternary amine groups and the protonated amine residues. In alkaline media, its net positive charge is maintained primarily due to the presence of the quaternary amine groups. Chang et al. reported on the preparation of TMC/glycerophosphate (GP) complex, which functioned as a pH-and thermoresponsive hydrogel (Chang et al., 2009). Furthermore, TMC has found utility in drug/gene delivery systems as a cationic stabilizer for colloidal nanoparticles/nanogels. Cationic TMC-based nanoparticles/nanogels have been explored as potential drug-delivery nanocarriers for targeted cancer therapy (Wang et al., 2010). These cationic nanocarriers exhibited mucoadhesive properties, thereby enhancing permeation across various biological barriers (e.g., blood-brain, intestinal, and nasal mucosal barriers). Additionally, they can facilitate intracellular uptake through electrostatic interaction with the negatively charged phosphate groups on cell membranes (Amidi et al., 2006; Sahni et al., 2008; Szabová et al., 2023; Thanou et al., 2001; Wang et al., 2010). Thus, TMC-based nanocarriers are promising for applications in drug/gene delivery.

Recently, we successfully developed redox-responsive nanogels, consisting of TMC periphery and crosslinked PHEMA core, so-called PHEMA-TMC nanogels (Lekjinda and Sunintaboon, 2023). These nanogels were synthesized through a green process using visible-light-induced surfactant-free emulsion polymerization (SFEP). However, the % cumulative drug release from these redox-responsive nanogels remained low (~60%).

Herein, we synthesized novel biocompatible multi-stimuli responsive PHEMA-TMC nanogels with pH- and light-dependent UCST-type thermoresponsive behavior. The synthesis was achieved through a facile and green synthetic method *via* SFEP using riboflavin (vitamin B2) as a photoinitiator and tertiary amine on TMC as a co-initiator. This technique was chosen due to its numerous advantages, including the use of water-based medium, a visible-light source, a non-toxic initiator system, and the absence of surfactants or other co-initiators. The thermoresponsive characteristics of the synthesized nanogels were found to be affected by factors, such as the degree of quaternization (DQ) of TMC, crosslinker content, and pH. This was characterized by dynamic light scattering (DLS), ^{1}H-NMR spectroscopy, and UV-vis spectrophotometry. For the purpose of investigating their potential chemotherapeutic applications, the selected PHEMA-TMC nanogel was used to encapsulate honokiol, a hydrophobic anti-cancer drug model derived from *Magnolia* plants. Additionally, for photothermal therapy, the nanogel was loaded with SCC, a biodegradable photothermal agent capable of triggering hyperthermia upon exposure to red-light. The characteristic of this dual loaded system, offering the combined benefits of photothermal therapy and chemotherapy was investigated.

2. Experimental section

2.1. Materials

Chitosan (CS) (molecular weight of 80–120 kDa, degree of deacetylation >85%, Bio21 Co. Ltd. Thailand), *N,N′*-methylene bisacrylamide (MBA, 99%, Sigma-Aldrich), *N*-methyl-2-pyrrolidone (NMP, >99.5%, RCI Labscan), riboflavin (RF, >98%, Sigma), sodium hydroxide (>99%, Merck), iodomethane (>99%, Merck), honokiol (>90%, Myskinrecipe Thailand), sodium copper chlorophyllin (SCC, >95%, Myskinrecipe Thailand) were used as received. 2-Hydroxyethyl methacrylate (HEMA, 97%, Sigma-Aldrich) was purified by passing it through a column packed with basic and neutral alumina absorbents. All organic solvents were of analytical grade, and were used without further purification.

Two LED lamps (model: LEDMR16D05W, type; daylight with 6500 K color temperature, Brand: GATA) were employed to initiate the visible-light-induced polymerization with a light intensity of 400 lumens for each lamp. Each lamp was positioned at the side of the reactor, maintaining a distance of approximately 1 cm between the reactor and the lamp. The two lamps were oriented perpendicularly to each other.

2.2. Synthesis of TMCs

TMCs with different DQs can be synthesized by the methylation reaction at room temperature using iodomethane (CH_3I) as a methylating agent (Fig. S1, supporting information) (Lekjinda and Sunintaboon, 2023). First, 20 g of CS was dispersed in 400 ml of NMP, and 200 ml of 9% (2.3 M) NaOH solution was slowly added. The mixture was then vigorously stirred by a magnetic stirrer for 30 min at 25 °C. Subsequently, 60 ml of CH_3I was added, and the reaction proceeded for 48 h. After the reaction was stopped, the mixture was precipitated using excess ethanol to obtain the TMC product in a solid form. Next, the product was dissolved in 500 ml of 20% (3.4 M) NaCl solution, and the solution was stirred magnetically at room temperature for 18 h to facilitate the exchange of iodide with chloride ions. After that, the TMC solution was dialyzed with distilled water for 3 days, followed by freeze-dried overnight to yield TMC powder. The DQ, and contents of other substitutions were deduced from the ^{1}H-NMR spectrum (as shown in Fig. S1b, supporting information). Based on this synthetic process, the obtained TMC had DQ around 20%.

TMCs with higher DQs can also be synthesized through additional methylation steps based on the previous methylation process. Briefly, in the process described above, before stopping the reaction, 30 ml of iodomethane, 100 ml of NMP, and 50 ml of 12% (3 M) NaOH solution were added to the mixture. The reaction mixture was then stirred at room temperature for another 48 h. If more DQ was required, the similar set of reagents at the same amounts was added again, and the reaction was continued for another 48 h before dialyzing and freeze-drying, as mentioned above, to obtain TMC products.

2.3. Synthesis of PHEMA-TMC nanogels

All nanogels were synthesized by the visible light-induced SFEP using RF as a photo-initiator (Lekjinda and Sunintaboon, 2023). Briefly, a typical procedure for synthesizing nanogel at a particular condition is described as follows. 10 g of 2.5 wt% TMC solution, 1 g (8 mmol) of HEMA, 16 mg (0.2 mmol) of $NaHCO_3$, 59 mg (0.4 mmol) of MBA crosslinker, and 1 g of 20 μM RF initiator solution were placed into a 100-ml three-neck water-jacketed reactor. The total weight of the mixture was adjusted to 25 g by adding distilled water. The mixture was then stirred at 25 °C under a nitrogen atmosphere in a dark room for 30 min. The polymerization reaction was initiated by irradiation from the two LED lamps (5 W) and under continuous magnetic stirring for 4 h. After that, the polymerization was stopped by turning off the light and exposing the product to the ambient atmosphere. The resulting latex product was purified by ultracentrifugation at 40,000 rpm for 1 h for 2 centrifugation-redispersion cycles. The dried nanogel was obtained by freeze-drying the purified latex overnight. Some portion of purified nanogel latex, and freeze-dried nanogel were kept in a refrigerator for further use.

2.4. Characterization of nanogels

Monomer conversion and solid content were determined using a gravimetric method (Lekjinda and Sunintaboon, 2023). The average diameter, polydispersity index (PDI), and ζ-potential of each nanogel were measured using a Zetasizer Nano-ZS (Malvern Instruments, UK). The cleaned nanogel latex was diluted in different buffer solutions (0.1 M acetate buffer pH 4, 4.5, 5, distilled water (pH 6), and 0.1 M Tris-HCl buffer (pH 9)) to achieve a concentration of approximately 1 mg/ml before measurement. For UCST experiments, the temperature of the nanogel latex was adjusted from 20 to 70 °C with a 2 °C increment. For the heating/cooling cycle experiment, the nanogel latex was subjected to three heating/cooling cycles between 20 and 70 °C. A variable temperature ^{1}H NMR spectrum of the nanogel in D_2O containing 1% CD_3COOD was recorded using a 500 MHz spectrometer (Bruker). The spectral intensities at different temperatures were calculated by comparing between the integrals of the solvent and polymer. The change in local micropolarity of the nanogel at different temperatures was assessed by UV-Vis spectrophotometer (Shimadzu UV-1800) with Nile red as a solvatochromic probe. A Nile red-loaded nanogel (~0.2% loading content) was incubated in acetate buffer at pH 5 at both 20 °C and 70 °C for 10 min before measuring the absorbance.

We used a transmission electron microscope (TEM, Hitachi HT7800) to visualize the morphology of the nanogels (Lekjinda and Sunintaboon, 2023). An equivalent point or a point of amine 's neutralization was determined from the acid-base titration curve between the nanogel latex (50 ml, 0.1% solid content) and 0.1 M NaOH. The curve illustrates the correlation between the pH of the nanogel dispersion and the volume of NaOH used.

2.5. Loading and release study

For honokiol loading into the selected PHEMA-TMC nanogel, 30 mg of the dried nanogel was dispersed in 2 ml of distilled water, and sonicated for 20 min. Then, 1 ml of honokiol solution in ethanol, which was varied as 3, 6, 12, and 24 mg/ml, was added to the dispersion. The dispersion was then magnetically stirred for 24 h. After that, ethanol was removed by a rotary evaporator. The resulting dispersion was centrifuged at 4000 rpm for 10 min to separate the unloaded honokiol, which precipitated at the bottom of the centrifuge tube. The amount of unloaded honokiol was quantified through its UV-Vis absorption at 293 nm by correlating those absorption data to the pre-established calibration curve. The honokiol loading content and efficiency were calculated according to the following equations.

$$\text{Loading content } (\%) = \frac{(\text{Wt. of honokiol in feed} - \text{Wt. of unloaded honokiol})}{\text{Wt. of the nanogel}} \times 100 \quad (1)$$

$$\text{Loading efficiency } (\%) = \frac{(\text{Wt. of honokiol in feed} - \text{Wt. of unloaded honokiol})}{\text{Wt. of honokiol in feed}} \times 100 \quad (2)$$

For encapsulating SCC, 30 mg of the dried nanogel or honokiol-loaded nanogel was dispersed in 2 ml of distilled water. Next, 1 ml of the SCC aqueous solution, which was varied as 3, 6, 12, and 24 mg/ml, was added to the dispersion and then magnetically stirred for 24 h. The dispersion was precipitated by ultracentrifugation at 40,000 rpm for 1 h for 2 centrifugation-redispersion cycles, to obtain the SCC-loaded nanogel or honokiol/SCC-loaded nanogel. The quantity of unloaded SCC in the supernatant was determined by measuring its UV-Vis absorption at 404 nm, and correlating the absorption data with the pre-established calibration curve.

To study the release of honokiol, 15 mg of dried honokiol/SCC co-loaded nanogel was dispersed in 3 ml water and placed in a dialysis membrane (molecular weight cut off:7000 Da). The membrane was then immersed in either 75 ml of PBS buffer solution at pH 7.4 or acetate buffer solution at pH 5 in the presence of 0.5% Tween 80. The incubation temperature was set at either 37 or 50 °C. At specific time intervals, 1 ml of the buffer medium was removed and quantified for the honokiol release. Simultaniously, 1 ml of fresh buffer solution was replenished into each flask under continuous incubation.

2.6. Red laser-induced photothermal study

SCC-loaded and honokiol/SCC-loaded nanogels were prepared by loading SCC and honokiol + SCC to the selected PHEMA-TMC nanogel with the same procedure as described earlier. Then, 0.5 ml of dispersions of each loaded nanogel in acetate buffer (pH 5) were prepared at various concentration levels (2.5, 5, and 10 mg/ml). These loaded nanogel dispersions were then exposed to red laser irradiation (635 nm, 1W/cm^2) for 10 min. During the process, a thermometer was used to intermittently measure the temperature of dispersions, and a thermal camera was used to capture their thermal images.

2.7. Cell viability

Human lung carcinoma cells (Calu-3) and Human lung fibroblast cells (MRC5) were cultured in Dulbecco's Modified Eagle Medium, and Ham's F-12 Medium (DMEM/F12, Gibco, Grand Island, NY, USA) supplemented with 10% FBS, 1% L-Glutamine, and 1% MEM Non-Essential Amino Acid solution (Gibco). The cells were grown at 37 °C under a 5% CO_2 atmosphere.

For cell biocompatibility, the MRC5 cells (10,000 cells/well) were seeded in 96-well plates and incubated with the empty nanogel for 24 h. DMSO (10% v/v) was used as a positive control. After incubation, CellTiter 96® AQ_{ueous} One Solution Reagent (Promega, USA, 20 μL) was added to each well, and cells were incubated at 37 °C with 5% CO_2 for 4 h. Absorbance was measured at 490 nm. The following equation was used to compute a percentage of cell viability:

$$\%\ \text{Cell viability} = \frac{O.D.\ of\ nanogel - treated\ cells - O.D\ of\ medium\ blank}{O.D.\ of\ untreated\ cells - O.D.\ of\ medium\ blank} \times 100 \quad (3)$$

For cell cytotoxicity, the Calu-3 cells (10,000 cells/well) were seeded in 96-well plates and incubated with the empty, SCC-loaded, honokiol-loaded, or honokiol/SCC co-loaded nanogels for 24 h. After incubation, CellTiter 96® AQ_{ueous} One Solution Reagent was added to each well, and cells were incubated at 37 °C with 5% CO_2 for 4 h. Absorbance was measured at 490 nm and percentage of cell viability was calculated using equation (3).

For evaluating the photothermal anti-cancer effect of honokiol/SCC co-loaded nanogel, Calu-3 cells were treated with honokiol/SCC co-loaded nanogel for 3 h at 37 °C, followed by exposure with a red-light laser (635 nm, 1W/cm^{-1}) for 2 min. The treated cells were then incubated at 37 °C for 21 h before determining the cell viability. The same procedure but without light irradiation was also conducted for comparison.

3. Results and discussion

3.1. Synthesis and characterization of PHEMA-TMC nanogels

In this current work, PHEMA-TMC nanogel can be synthesized by the visible light-induced SFEP using RF/TMC as a redox photoinitiating system and MBA as a crosslinker (see Fig. 1a). Tertiary amine moieties in TMC can play an essential role by working as a co-initiator alongside the RF initiator to generate active free radicals that initiate the polymerization process. The mechanism of free-radical generation and nanogel formation has been described elsewhere (Lekjinda and Sunintaboon, 2023; Ratanajanchai et al., 2013). Furthermore, the quaternary amine groups in TMC contribute to the colloidal stabilization of the resulting cationic nanogels. These groups facillitate the loading of anionic molecules (e.g., dye), and enhance cell adhesion through electrostatic interaction. During the SFEP process, as PHEMA chains grow to a critical chain length on TMC backbone, amphiphilic TMC-graft-PHEMA structures form. These structures possess the ability to self-assemble into the core-shell structure, having crosslinked PHEMA core and TMC shell. This assembly is driven by interactions between the hydrophobic PHEMA chains crosslinked by MBA crosslinker and the hydrophilic TMC chains. The crosslinked PHEMA core forms a three-dimensional network, that provides structural stability, enables the encapsulation of hydrophobic molecules (e.g., drug), and facilitates the absorption of hydrophilic molecules (e.g., water).

In this work, TMC was initially synthesized through a methylation method using native CS as the starting material. This reaction primarily results in *N*-trimethylation and *N*-dimethylation, which introduce quaternary amine and tertiary amine moieties to the CS structure, respectively. The contents of *N*-trimethylation (degree of quaternization, DQ) and *N*-dimethylation (degree of dimethyla-

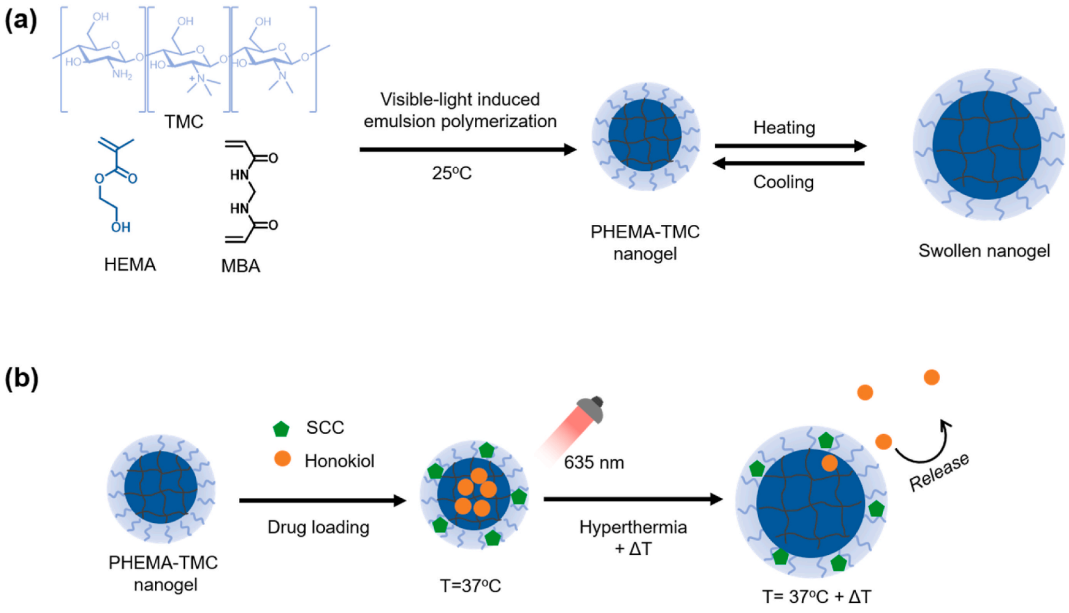

Fig. 1. Schematic illustration of (a) synthesis of PHEMA-TMC nanogel and its thermo-responsive behavior and (b) co-loading of SCC and honokiol in PHEMA-TMC nanogel and red light-triggered release of honokiol. (For interpretation of the references to color in this figure legend, the reader is referred to the Web version of this article.)

tion, DM) were determined through ^{1}H-NMR spectroscopic analysis, and their respective contents are shown in Table S1 (supporting information). Three types of synthesized TMC were denoted as TMC20, TMC45, reflecting their approximate DQ values of 20, 45, and 65%, respectively. It can also be seen from the analysis of these three TMCs that as the DQ increased from 20 to 64%, the DM decreased from 57 to 7%.

The effect of TMC with varying DQs and DMs on the polymerization performance and characteristics of the resulting nanogels was firstly investigated. After conducting polymerization with different TMCs, the polymerization kinetics, percent conversions and solid contents were determined, as shown in Fig. 2a and Table 1. The synthesized nanogels were designated as PHEMA-TMC20, PHEMA-TMC45, and PHEMA-TMC65, when using TMC20, TMC45, and TMC65, respectively. Among three types of TMC, TMC20 and TMC45 caused the better polymerization performance with high percent conversions (~90%), and solid contents (~5%) of the nanogel latex products. In contrast, TMC65 gave lower polymerization performance with a percent conversion of ~70%, and a solid content of ~4%. This decreased polymerization performance by TMC65 could be caused by a lower DM content (only 7%) in comparison to the DMs of TMC20 and TMC45 (Table S1). This result emphasizes the significant role played by the tertiary amine in TMC as a co-initiator to generate active free radicals in this photopolymerization system. In addition, the type of TMC also affected the characteristics of the resulting nanogels. As evidenced in Fig. 2c and Table 1, the nanogels synthesized with different TMCs had sizes between 116 and 140 nm with narrow size distributions (PDIs <0.2) (Xu et al., 2022). Notably, size tended to decrease with increasing DQ. Their ζ-potentials were not much different (23–24 mV). However, such positive values reflect the cationic surface characteristic because of the presence of TMC on the nanogels' periphery layer. Also, the changes in both size and ζ-potential values of the nanogels upon changing pH in the range of 4–10 are displayed in Fig. S2 (supporting information). It can be seen that the pH variations within this range influenced the colloidal stability and cationic characteristic of the nanogels. When increasing pH from 4 to 6, ζ-potentials of all nanogels decreased in magnitude, shifting from around 33-36 mV–10 mV. Upon further increasing pH from 6 to 10, ζ-potentials of PHEMA-TMC45 and PHEMA-TMC65 nanogels remained relatively constant (~10 mV). In contrast, the ζ-potential of PHEMA-TMC20 nanogel decreased and approached zero at pHs 9–10, accompanied by some precipitation. Based on the results from Fig. S2, it could be said that TMC shell can maintain the cationic characteristic across a wider pH range due to its permanent cationic quaternary amine moieties. In addition, the nanogels prepared with TMC having higher DQ appeared to exhibit a greater capacity to retain their cationic nature. In Fig. 2e and g, FTIR spectroscopic analysis indicates an increasing intensity of $-CH_3$ groups at 2950 cm^{-1} with higher DQ, confirming the presence of TMC with varying DQ in the synthesized nanogels. In Fig. 3a, the TEM image confirms the core-shell morphology of the nanogels, aided by phosphotungstic acid staining. Fig. 3b shows the imperfectly spherical morphology of PHEMA-TMC45 nanogel, as visualized by FE-SEM. It can be seen that the sizes of the nanogels from electron microscope (Fig. 3) and DLS (Fig. 2c–d) are different. SEM/TEM images depict the nanogels in a dried state, while DLS determine the size of the nanogels when dispersed in aqueous medium. Those from DLS appear to be larger because the nanogels can absorb a large amount of water into their structure, causing them to swell in an aqueous medium. Since PHEMA-TMC45 nanogel can be synthesized with a high % conversion, solid content, and colloidal stability over a wide pH range, its polymerization condition was selected as the optimal condition for further varying MBA concentration in the next section.

In this section, the concentration of MBA was further varied to 2.5 and 10 mol%, and the results were compared with those obtained under the optimal condition (5 mol% MBA) as previously discussed. When considering the effect of MBA concentration, it was

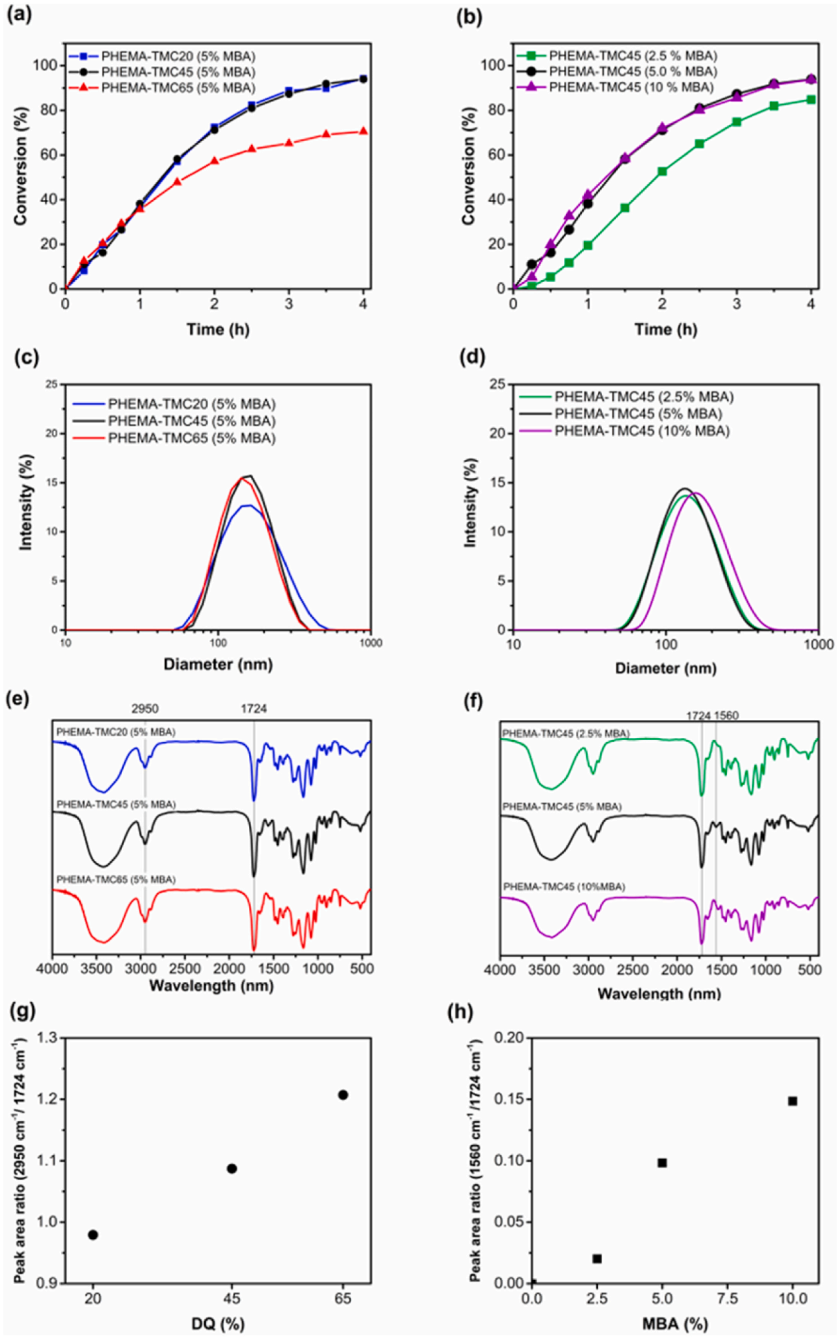

Fig. 2. % Conversion-time plots from the polymerization systems prepared by using (a) TMC with different DQs, and (b) various MBA contents; Hydrodynamic diameters of PHEMA-TMC nanogels prepared by using (c) TMC with different DQs, and (d) various MBA contents; FTIR spectra of PHEMA-TMC nanogels synthesized from (e) TMC with different DQs, and (f) various MBA contents; (g) the relationship between peak area ratio of ν(C-H, 2950 cm^{-1})/ν(C = O, 1724 cm^{-1}) of PHEMA-TMC nanogels synthesized from TMC with different DQs; (h) the relationship between peak area ratio of ν(amide II, 1560 cm^{-1})/ν(C = O, 1724 cm^{-1}) of PHEMA-TMC nanogels synthesized from various MBA contents.

found that the percent conversion of PHEMA-TMC45 nanogel with 2.5 mol% MBA was ~77%, while those with 5 and 10 mol% MBA were higher, reaching up to ~90%. The polymerization using 2.5% MBA had slightly lower polymerization performance as shown in Fig. 2b. This lower final conversion and slow polymerization could be influenced by the reactivity ratio between the HEMA monomer and the MBA crosslinker (Liu et al., 2019). Furthermore, the size of prepared nanogels tended to increase from 115 to 164 nm when increasing MBA from 2.5 to 10% (Fig. 2d, Table 1). The FTIR spectroscopic evidence qualitatively confirmed the presence of amide II bond at 1560 cm^{-1} from MBA in the synthesized nanogels (Fig. 2f and h). These results indicate that the concentration of MBA crosslinker also influences on the emulsion polymerization process and the characteristics of the synthesized nanogels.

Table 1
Percent conversions, solid contents, average diameters, PDIs, ζ-potentials, and volume ratios over two temperature ranges: 20 °C–70 °C and 37 °C–50 °C.

Materials	Conversion (%)	Solid content (%)	Size[a] (nm)	PDI[a]	ζ-potential[a](mV)	Volume ratio V_{20}/V_{70}	Volume ratio V_{37}/V_{50}
Effect of DQ on TMC							
PHEMA-TMC20 (5% MBA)	91 ± 1	5.0 ± 0.1	140 ± 7	0.101 ± 0.012	23 ± 7	1.3	1.0
PHEMA-TMC45 (5% MBA)	90 ± 2	4.9 ± 0.2	124 ± 8	0.088 ± 0.001	24 ± 0	1.8	1.2
PHEMA-TMC65 (5% MBA)	70 ± 8	3.9 ± 0.1	116 ± 1	0.077 ± 0.001	23 ± 2	1.3	1.0
Effect of MBA concentration							
PHEMA-TMC45 (2.5% MBA)	77 ± 9	4.3 ± 0.4	115 ± 1	0.075 ± 0.006	23 ± 6	1.0	1.0
PHEMA-TMC45 (10% MBA)	92 ± 6	5.2 ± 0.2	164 ± 43	0.108 ± 0.001	29 ± 2	2.0	1.2

[a] Measured in acetate buffer, pH 5 at 25 °C.

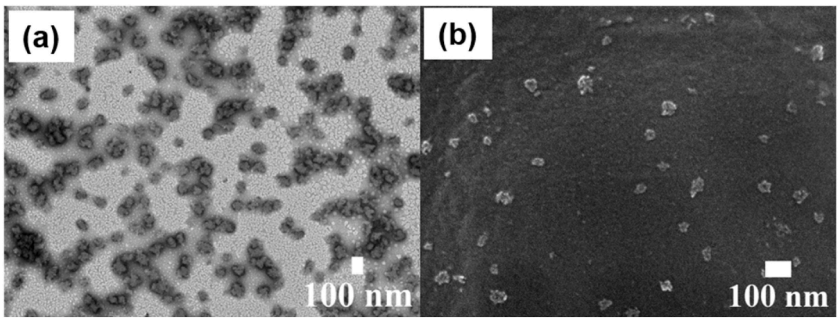

Fig. 3. (a) TEM image with phosphotungstic acid staining of PHEMA-TMC44 (5% MBA) nanogel, (b) FE-SEM image of PHEMA-TMC44 (5% MBA) nanogel.

3.2. Thermo-responsiveness of PHEMA-TMC nanogels

The introduction of cationic comonomers, particularly those with quaternary amines and protonated tertiary amines, to PHEMA can lower its UCST to below 100 °C (Longenecker et al., 2011). They proposed that quaternary amines and protonated tertiary amines disrupt the hydrogen bonding interactions among the PHEMA chains themselves, especially from the hydroxyl groups, while enhancing the polymer-solvent hydrogen bonding interaction, thus increasing its swelling ability at temperatures above UCST. Therefore, we assessed the thermoresponsiveness of PHEMA-TMC nanogels upon a variation of dispersion pH. Considering that the nanogels are crosslinked colloidal particles, their thermo-responsiveness was monitored through size/volume changes with temperature, instead of the soluble-insoluble transition seen in PHEMA or its copolymer solution. For this assessment, we selected the representative PHEMA-TMC45 nanogel (5 mol%) and investigated their thermoresponsive behavior at 20–70 °C. Before measurement, the dried nanogel was dispersed with distilled water and its pH was adjusted to be in the range of 4–6. We also investigated the nanogel characteristics at an extremely basic pH (pH 9) for comparison purpose. The changes of the nanogel's size in different pHs are displayed in Fig. 4a. It can be seen that the nanogel displayed size changes above 30 °C when its dispersion pH was at pHs 4.5 and 5, indicating pH-dependent thermoresponsive behavior. The volume ratios (V_{70}/V_{20}) were also calculated (Fig. 4b), suggesting that pHs 4.5 and 5 induced relatively greater thermoresponsiveness compared to other pHs. Fig. 4c reveals the equivalent point of the nanogel at pH 5.8, referring to the pH where all amine groups become neutral. Below this pH, the nanogel's surface had protonated amines, leading to a slight increase in size and ζ-potential (Fig. 4d). However, during heating, the increase in hydrodynamic size primarily resulted from PHEMA core swelling (Fig. 4e). Based on the previous report by Longenecker et al., PHEMA copolymerized with cationic monomers displayed the UCSTs around 80 °C (Longenecker et al., 2011). Surprisingly, our work showed that the PHEMA-TMC45 nanogel exhibited a UCST-type size change within a lower temperature range, covering the physiological temperature range. Such behavior would stem from the disruption of hydrogen bonds among PHEMA hydroxyl groups due to the combined effects of amine-containing TMC and amide-bearing MBA crosslinker. A similar work by Yang et al. (2018) reported larger volume ratios of poly(*N*-acryloyl glycinamide) (PNAGA) nanogel, around 2.7–4.1 in the 20–70 °C temperature range, compared to our nanogel in this current work. However, our PHEMA-TMC nanogel possessed a dual response to temperature and pH, making it intriguing for precisely controlled release application. The PHEMA-TMC nanogel can encapsulate anticancer drugs, releasing them under specific conditions, such as acidic environments (e.g., lysosomal at a pH of 4.5–5 (Chen et al., 2020)), and elevated temperature environments (e.g., hyperthermia treatment at 50 °C (Chang and Tsai, 2018)). The result in Fig. 4b displayed the nanogel's volume ratios of around 1.2 at pH 4.5–5 and 37–50 °C, representing the normal body temperature-hyperthermia range, indicating its ability to swell under these specific conditions.

We then analyzed the thermoresponsiveness of the PHEMA-TMC nanogels that were synthesized using TMC with different DQs and MBA concentrations. This analysis was conducted at pH 5 and within the temperature range of 20–70 °C. The thermoswelling behaviors of these nanogels are illustrated in Fig. 5a–b. Among the nanogels based on the three distinct TMC compositions, both PHEMA-TMC20 and PHEMA-TMC65 nanogels displayed the changes in their diameters at the volume phase transition temperature around 60 °C. In contrast, PHEMA-TMC45 nanogel exhibited an abrupt diameter change around 30 °C. This distinctive behavior can be related to the optimal proportions of quaternary amines and protonated tertiary amine, which play a role in disrupting the hydro-

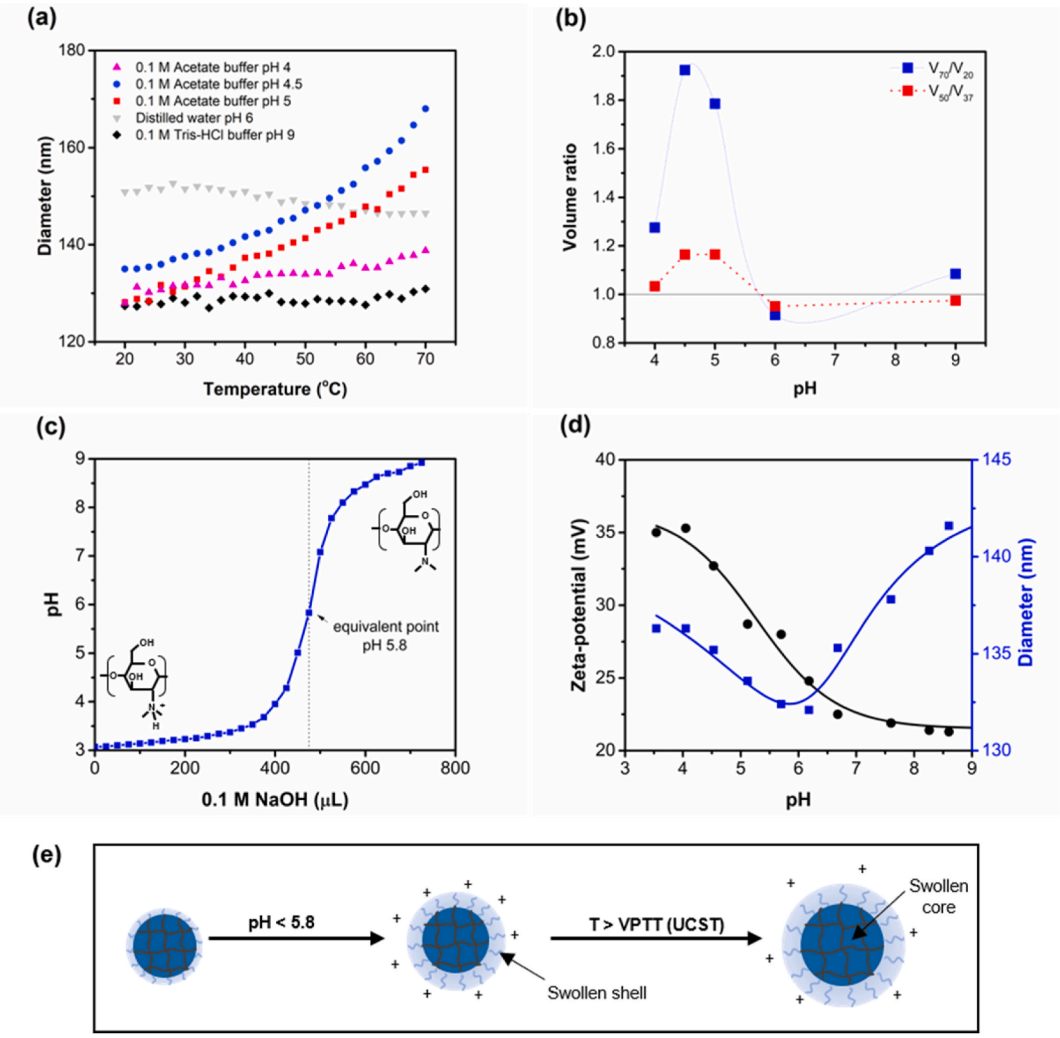

Fig. 4. (a) Changes of PHEMA-TMC45 (5% MBA) nanogel's diameter in different pH media; (b) pH-Dependent volume ratios at T_{70}/T_{20} and T_{50}/T_{37} of PHEMA-TMC45 (5% MBA) nanogel; (c) Equivalent point from the titration curve of PHEMA-TMC45 (5% MBA) nanogel with 0.1 M NaOH; (d) Hydrodynamic diameter and ζ-potential of PHEMA-TMC45 (5% MBA) nanogel as a function of pH; and (e) Schematic illustration of the change in size of nanogel in acidic pH (pH < 5.8) and elevated temperature (T > volume phase transition temperature (VPTT)).

gen bonding interactions among PHEMA chains. Since PHEMA-TMC45 nanogel undergoes size changes across the physiological temperature range, we selected its polymerization condition as the base for further variation.

Next, we analyzed the effect of MBA concentration on the thermoresponsiveness. MBA concentration was varied as 2.5, 5, and 10% for synthesizing the respective PHEMA-TMC45 nanogels. The thermoresponsive behaviors of these nanogels are shown in Fig. 5b. PHEMA-TMC45 nanogels with 5 and 10% MBA exhibited similar thermoresponsive behaviors, characterized by broad swelling transitions, leading to increased diameters within the temperature range of 20–70 °C. In contrast, PHEMA-TMC45 nanogel with 2.5% MBA did not show a significant change in diameter within the same temperature range. Therefore, MBA concentration significantly influences the thermoresponsiveness of the PHEMA-TMC45 nanogel.

Moreover, the diameters of PHEMA-TMC45 nanogels synthesized with 5 and 10% MBA were determined through a heating/cooling process between 70 and 20 °C. It can be seen from Fig. 5c that both nanogels exhibited reversible size changes for up to three heating/cooling cycles. Nonetheless, there was a slight degree of incomplete recovery in the nanogels' size, particularly during the cooling process. This phenomenon could be attributed to a hysteresis effect (see Fig. S3). Here, hysteresis refers to the disparity in phase transition observed during heating and cooling. This can be influenced by various factors, including the cooling rate (Augé et al., 2018) or homogeneity of the network (Audureau et al., 2021; Tran et al., 2020). As schematically illustrated in Fig. 5d, the reversible swelling and shrinking of PHEMA chains are driven by hydrogen bonding interaction. At higher temperatures, solvent molecules can penetrate into the polymer chains, disrupting their intermolecular forces and causing the nanogel to swell. This ability of the nanogel to undergo reversible swelling/shrinking in response to temperature changes suggests its potential ability in temperature-triggered drug release application.

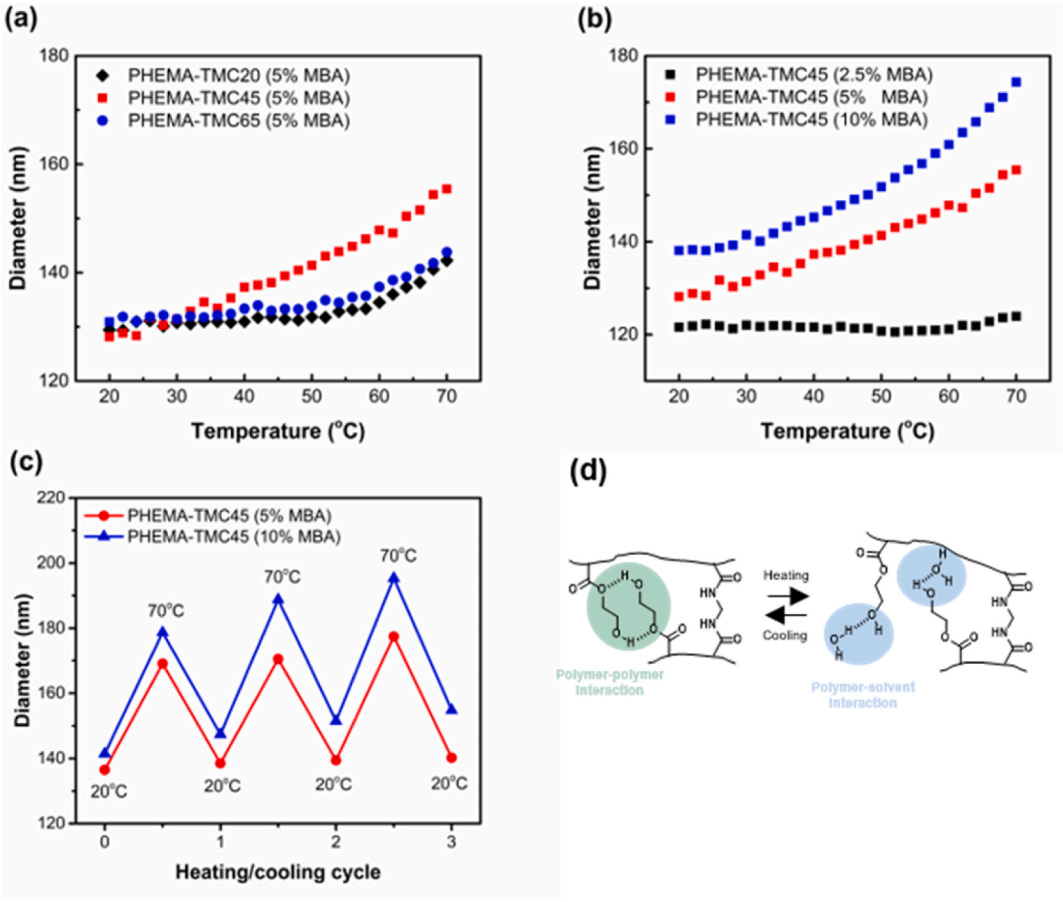

Fig. 5. (a) The change of UCST behavior at different DQs on TMCs, (b) The change of UCST behavior at different MBA contents, (c) Reversible deswelling/swelling behavior under the heating/cooling process, and (d) Schematic illustration of the reversible UCST-type process of PHEMA.

The evidence for the change in nanogel size with temperature was also supported by ^{1}H-NMR spectroscopy (Fig. 6a–b). The integration of methylene protons of PHEMA in the PHEMA-TMC45 (5% MBA) nanogel at 3.8–4.2 ppm was intensified upon heating. This observation could be caused by the disruption of polymer-polymer hydrogen bonding, leading to increased chain mobility and subsequently amplified proton signals. Additionally, the change of local polarities of the PHEMA-TMC45 (5% MBA) nanogel at various temperatures was traced with the assistance of the Nile red as a solvatochromic dye (Fig. 6c) incorporated into the nanogel. Upon heating to 70 °C, the redshifted UV-Vis absorption of Nile red was observed at the higher wavelength of 577 nm. This shift indicates the increase in local polarities within the nanogel as a result of heightened interaction between PHEMA chains and the surrounding medium due to hydrogen bonding cleavage (Hornum et al., 2020).

3.3. Photothermal property

We selected PHEMA-TMC45 nanogel (5% MBA) as a carrier to study its photothermal responsiveness and its potential for hydrophobic drug release. The drug release would be further developed to allow the nanogel to function as a carrier for photothermal/chemotherapy applications. In the initial step, the PHEMA-TMC45 nanogel was co-loaded with anionic SCC in the TMC periphery layer through electrostatic interactions and hydrophobic honokiol in the PHEMA network core. This nanogel system is anticipated to enable photothermal/chemotherapy due to the hyperthermia induced by the SCC's light absorption, followed by thermo-swelling of the nanogel, expecting to trigger the release of encapsulated honokiol for chemotherapy. The characteristics of the nanogel, such as size, encapsulation efficiency, and loading content are summarized in Table S2. In the honokiol/SCC co-loaded nanogel, the loading contents were 14% for honokiol and 16% for SCC. TEM analysis confirmed the spherical morphology of nanogel after co-loading (Fig. S4).

We investigated the photo-induced hyperthermia effect of the honokiol/SCC co-loaded PHEMA-TMC45 (5% MBA) nanogel through red laser irradiation (635 nm, 1 W cm^{-2}). The temperature change during irradiation was measured by both a thermal camera (Fig. 7a) and a thermometer (Fig. 7b). Both sets of results revealed that the presence of SCC in the honokiol/SCC co-loaded PHEMA-TMC45 nanogel caused the proportional increase in temperature. For example, utilizing the nanogel at a concentration of 10 mg/mL and subjecting it to 6 min of laser irradiation caused the temperature to rise from 30 to 45 °C. This observation emphasizes the hyperthermic property of the co-loaded nanogel, indicating its potential for applications in hyperthermia therapy.

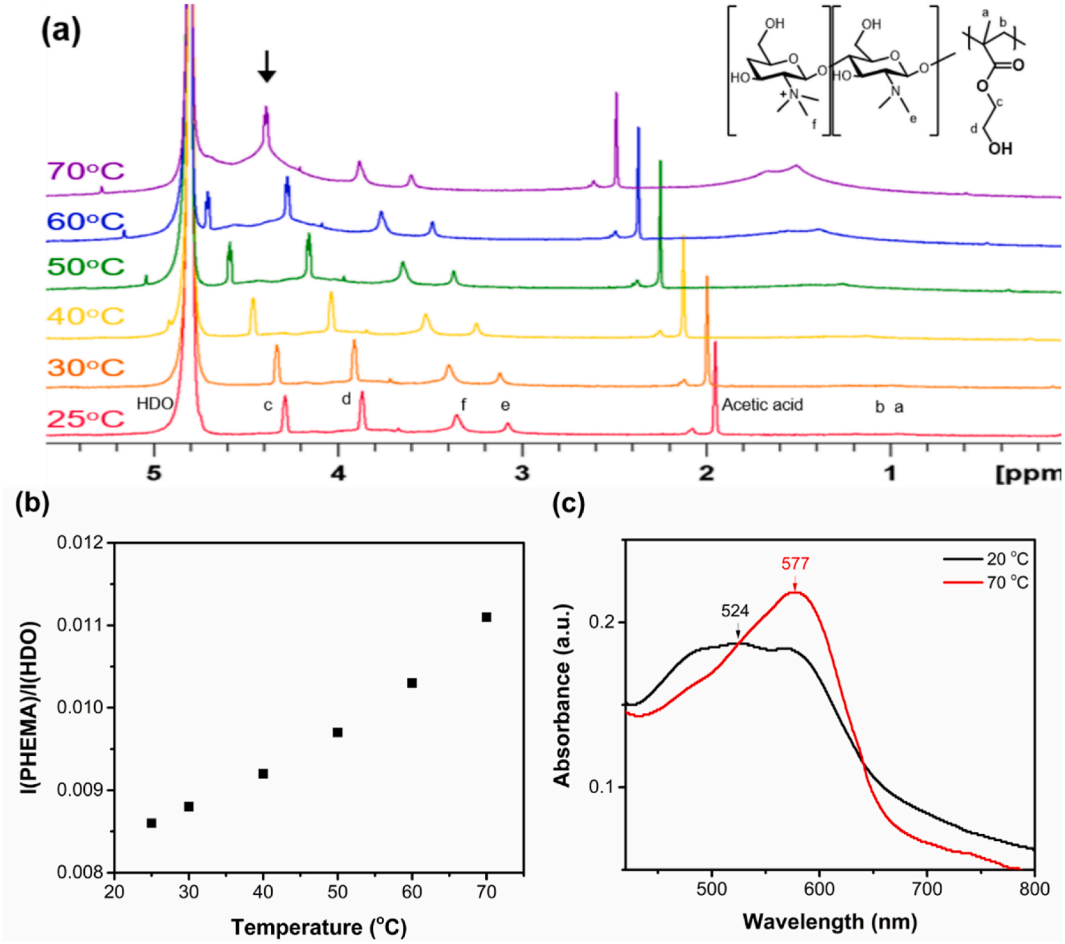

Fig. 6. (a) ^{1}H-NMR spectra of PHEMA-TMC45 (5% MBA) nanogel in D_2O containing 1% CD_3COOD at various temperatures. (b) The corresponding integrated signal intensity of PHEMA at different temperatures compared with the solvent (HOD) signal. (c) Absorption spectra of Nile red-loaded PHEMA-TMC45 (5% MBA) nanogel at 20 and 70 °C. (For interpretation of the references to color in this figure legend, the reader is referred to the Web version of this article.)

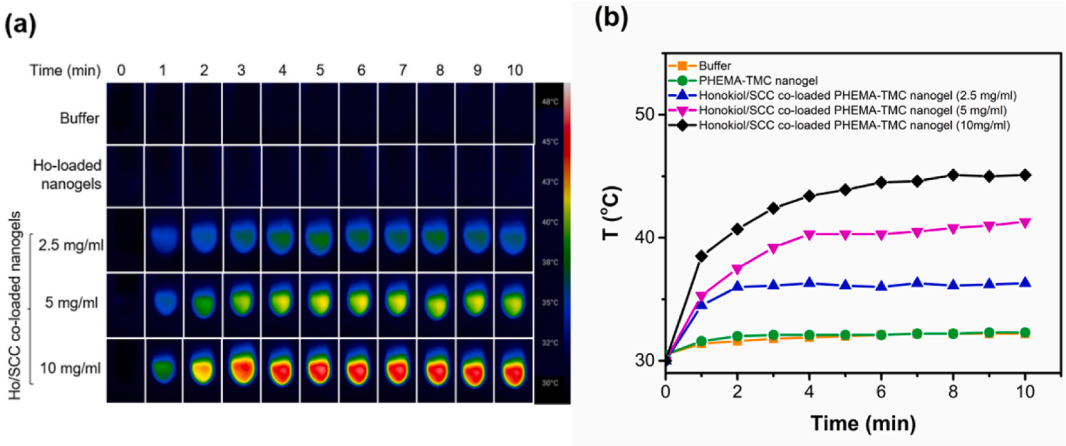

Fig. 7. Photothermal study of honokiol/SCC co-loaded PHEMA-TMC45 (5% MBA) nanogel using (a) a thermal camera and (b) a thermometer.

3.4. In vitro drug release

We performed the *in vitro* release studies of honokiol from the honokiol/SCC co-loaded PHEMA-TMC45 (5% MBA) nanogel at two different temperatures (37 °C and 50 °C) and two pH levels (5 and 7.4). The release profiles are shown in Fig. 8a. The fastest honokiol release and highest % cumulative release of ~87% were observed at 50 °C/pH 5, followed by 37 °C/pH 5, 50 °C/pH 7.4, and 37 °C/pH

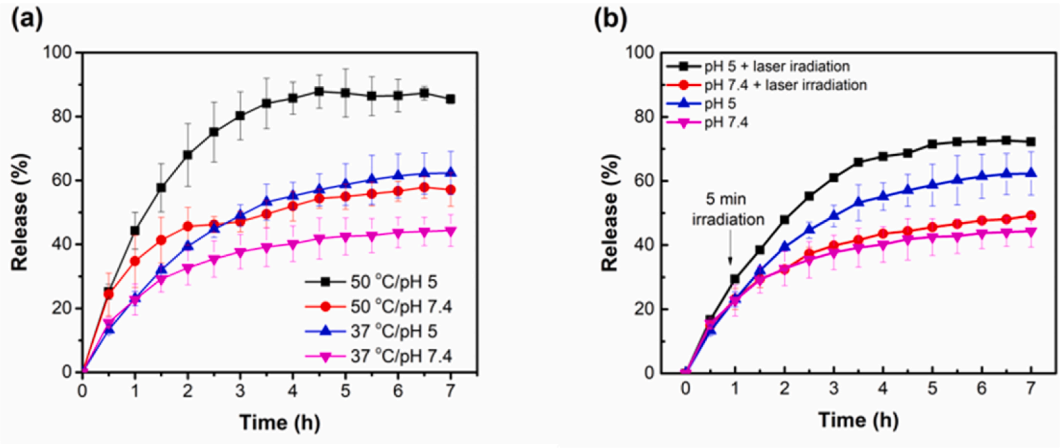

Fig. 8. (a) *In vitro* release of honokiol from honokiol/SCC co-loaded PHEMA-TMC45 (5% MBA) nanogel. (b) *In vitro* release under 635 nm laser irradiation.

7.4. These results suggest that the nanogel can swell and cause the release of encapsulated honokiol at high temperatures and under acidic environment. Furthermore, we investigated the effect of light irradiation on the honokiol release at the same temperature but varying pH conditions. The incubation temperature for this study was at 37 ˚C. As shown in Fig. 8b, the fastest honokiol release was observed at pH 5 with laser irradiation, indicating that the co-loaded nanogel could release the encapsulated honokiol by a photothermal trigger and in the acidic environment. The absence of a green appearance in the buffer solutions across all tested conditions in this release study assures the negligible leaching of SCC from the nanogel (Arimoto-Kobayashi et al., 1997). Based on these results, it was concluded that the honokiol/SCC co-loaded PHEMA-TMC45 nanogel can respond to red laser light irradiation, temperature changes, and pH variations, making it a promising candidate for controlled drug release.

We fitted the release data from Fig. 8a into different kinetic models (Fig. S5, Table S3). The release of honokiol under the conditions of 37 ˚C/pH 7.4 and 50 ˚C/pH 7.4 were fitted well with Korsmeyer-peppas model. Their release exponent (n) values were obtained between 0.43 and 0.85, indicated the mechanism of drug release as anomalous (non-Fickian) transport. Conversely, the condition of 37 ˚C/pH 5 was fitted with Higuchi model, indicating the release of drug from the nanogel based on Fickian diffusion. However, the condition of 50 ˚C/pH 5 was matched with zero-order, indicating the drug's release from the nanogel in swollen-state depending on the drug's concentration. It was noticed that the changes in environmental stimuli (pH, temperature) can influence the change in the release kinetic model, which is a key characteristic of multi-stimuli responsive nanogels for controlled-release drug delivery.

3.5. Biocompatibility

For intranasal drug delivery application, the characteristics of the formulation, such as size, shape, PDI, zeta-potential, encapsulation efficiency, were evaluated. Based on all of the results, the nanogel is spherical with low PDI, having size lower than 200 nm, and possessing positively charged surface, indicating that this nanogel is preferable for transmucosal intranasal drug delivery (Costa et al., 2021). Moreover, the advantages of this nanogel include their versatility in loading both hydrophobic and hydrophilic therapeutic agents, high loading content, and the ability to control release under specific conditions. We assessed the viability of the empty nanogel against MRC5 (human lung fibroblast) normal cell lines using MTS assay, as shown in Fig. S6. The high cell viability ($>80\%$) confirmed the biocompatibility of the nanogel with normal cells. The excellent biocompatibility is a result of using biocompatible polymers and the green synthesis method without toxic reagents.

3.6. In vitro toxicity

We conducted a study on the cell viability of loaded- and unloaded-PHEMA-TMC45 (5% MBA) nanogels against Calu-3 cell (human lung cancer cell) line through MTS assay for 24 h incubation time. In Fig. 9a, both the empty PHEMA-TMC45 nanogel and the SCC-loaded nanogel showed excellent biocompatibility without decreasing the percentage of cell viability. In contrast, the cell viability of the honokiol-loaded nanogel and the honokiol/SCC co-loaded nanogel exhibited a concentration-dependent decline, suggesting the dose-dependent chemotherapeutic efficacy. These results highlight the potential of honokiol as an effective anti-cancer drug for chemotherapy. Furthermore, we compared the cell viability of honokiol/SCC co-loaded PHEMA-TMC45 nanogel with and without red light irradiation (Fig. 9b). The non-irradiated state was modified by 2 min of red-light laser treatment. Without irradiation, the cell viability decreased to ~80% at 250 μg/ml and ~50% at 500 μg/ml, primarily due to the chemotherapy effect driven by honokiol. However, after irradiation, the cell viability plummeted to ~20% for both 250 and 500 μg/ml treatments. This significant decrease in cell viability post-irradiation can be attributed to the combination of chemotherapeutic and photothermal effects. Thus, these nanogels exhibit promising potential for combined chemotherapy and photothermal therapy.

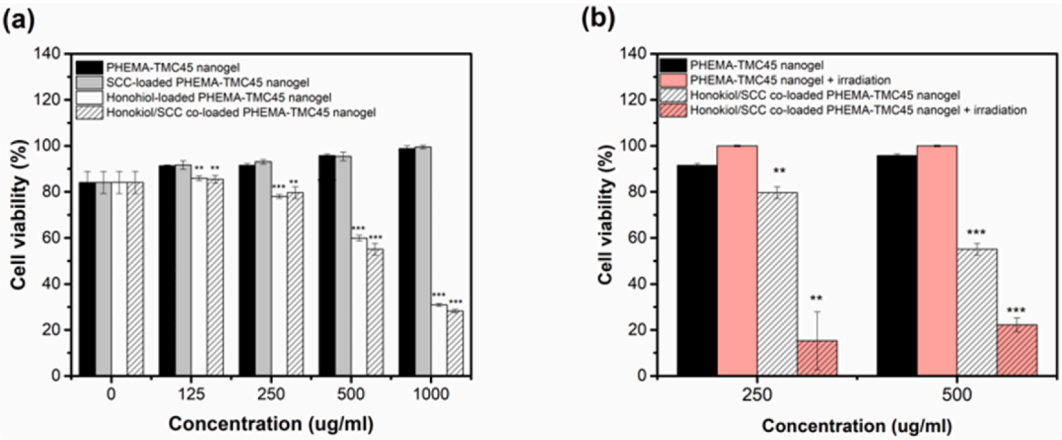

Fig. 9. (a) The viability of Calu-3 cells at different concentrations of nanogels: free PHEMA-TMC45, SCC-loaded PHEMA-TMC45, honokiol-loaded PHEMA-TMC45, and honokiol/SCC co-loaded PHEMA-TMC45 nanogels, (b) cell viability under with/without 635 nm red laser irradiation (n = 3, *: $p < 0.05$, **: $p < 0.01$, ***P: <0.001). (For interpretation of the references to color in this figure legend, the reader is referred to the Web version of this article.)

4. Conclusion

Multi-stimuli responsive PHEMA-TMC core-shell nanogels were fabricated through visible light-induced surfactant-free emulsion polymerization using riboflavin as a photo-initiator. Their UCST-type thermoresponsive property was optimized by varying the type of TMC, and MBA concentration. At the optimal condition, PHEMA-TMC45 nanogel was synthesized using TMC with 45% DQ and 5% MBA crosslinker. Also, the nanogel exhibited the reversible UCST-type volume phase transition at >30 °C in acidic media (pH 4.5–5). The nanogel was utilized to encapsulate SCC as a photo-absorbing agent and honokiol as a hydrophobic anticancer model drug were loaded to the nanogel, causing the concentration-dependent photothermal property and the enhanced release of honokiol under red light irradiation. The release mechanism is proposed due to the photothermal and thermoresponsive property of the nanogel, which result in its swelling and subsequent release of the encapsulated honokiol. Consequently, the PHEMA-TMC nanogel, as developed in this work, exhibits a significant potential as a could be potentially useful nanocarrier for the application in synergistic cancer therapy.

Author statement

This work was financially supported by the Royal Golden Jubilee (RGJ) Ph.D. Programme (Grant No. Ph.D. 0122/2558), Thailand Science Research and Innovation (TSRI), and National Research Council of Thailand (NRCT). This work was also supported by the Basic Science Research Program and Brain Pool program of the National Research Foundation (NRF), funded by the Korean government (MOE and MSIT) (2021H1D3A2A02045561).

Declaration of competing interest

The authors declare that they have no known competing financial interests or personal relationships that could have appeared to influence the work reported in this paper.

Data availability

Data will be made available on request.

Acknowledgments

This work was financially supported by the Royal Golden Jubilee (RGJ) Ph.D. Programme (Grant No. Ph.D. 0122/2558), Thailand Science Research and Innovation (TSRI), and National Research Council of Thailand (NRCT). This work was also supported by the Basic Science Research Program and Brain Pool Program of the National Research Foundation (NRF), funded by the Korean Government (MOE and MSIT) (2021H1D3A2A02045561).

Appendix A. Supplementary data

Supplementary data to this article can be found online at https://doi.org/10.1016/j.scp.2023.101290.

References

Amidi, M., Romeijn, S.G., Borchard, G., Junginger, H.E., Hennink, W.E., Jiskoot, W., 2006. Preparation and characterization of protein-loaded N-trimethyl chitosan nanoparticles as nasal delivery system. J. Contr. Release 111, 107–116. https://doi.org/10.1016/j.jconrel.2005.11.014.

Arimoto-Kobayashi, S., Harada, N., Tokunaga, R., Odo, J., Hayatsu, H., 1997. Adsorption of mutagens to chlorophyllin–chitosan, an insoluble form of chlorophyllin. Mutat. Res. Fund Mol. Mech. Mutagen 381, 243–249. https://doi.org/10.1016/S0027-5107(97)00188-7.

Audureau, N., Veith, C., Coumes, F., Nguyen, T.P.T., Rieger, J., Stoffelbach, F., 2021. RAFT-polymerized N-Cyanomethylacrylamide-Based (Co)polymers exhibiting tunable UCST behavior in water. Macromol. Rapid Commun. 42, 2100556. https://doi.org/10.1002/marc.202100556.
Augé, A., Camerel, F., Benoist, A., Zhao, Y., 2020. Near-infrared light-responsive UCST-nanogels using an efficient nickel-bis(dithiolene) photothermal crosslinker. Polym. Chem. 11, 3863–3875. https://doi.org/10.1039/D0PY00567C.
Augé, A., Fortin, D., Tong, X., Zhao, Y., 2018. Nanogel-like UCST triblock copolymer micelles showing large volume expansion before abrupt dissolution. Polym. Chem. 9, 4660–4673. https://doi.org/10.1039/C8PY00960K.
Chang, R., Hsu, C.-F., Tsai, W.-B., 2018. Fabrication of chlorophyll-incorporated nanogels for potential applications in photothermal cancer therapy. ACS Omega 3, 16057–16062. https://doi.org/10.1021/acsomega.8b01689.
Chang, R., Tsai, W.-B., 2018. Fabrication of photothermo-responsive drug-loaded nanogel for synergetic cancer therapy. Polymers 10. https://doi.org/10.3390/polym10101098.
Chang, Y., Xiao, L., Du, Y., 2009. Preparation and properties of a novel thermosensitive N-trimethyl chitosan hydrogel. Polym. Bull. 63, 531–545. https://doi.org/10.1007/s00289-009-0103-6.
Chen, R., Jäättelä, M., Liu, B., 2020. Lysosome as a central hub for rewiring PH homeostasis in tumors. Cancers 12. https://doi.org/10.3390/cancers12092437.
Costa, C.P., Moreira, J.N., Sousa Lobo, J.M., Silva, A.C., 2021. Intranasal delivery of nanostructured lipid carriers, solid lipid nanoparticles and nanoemulsions: a current overview of in vivo studies. Acta Pharm. Sin. B 11, 925–940. https://doi.org/10.1016/j.apsb.2021.02.012.
Hornum, M., Reinholdt, P., Zaręba, J.K., Jensen, B.B., Wüstner, D., Samoć, M., Nielsen, P., Kongsted, J., 2020. One- and two-photon solvatochromism of the fluorescent dye Nile Red and its CF3, F and Br-substituted analogues. Photochem. Photobiol. Sci. 19, 1382–1391. https://doi.org/10.1039/D0PP00076K.
Hu, C., Xu, W., Conrads, C.M., Wu, J., Pich, A., 2021. Visible light and temperature dual-responsive microgels by crosslinking of spiropyran modified prepolymers. J. Colloid Interface Sci. 582, 1075–1084. https://doi.org/10.1016/j.jcis.2020.08.081.
Jia, Y.-G., Yu, Q., Ma, Z., Zhang, M., Zhu, X.X., 2017. Tunable upper critical solution temperatures for acrylamide copolymers with bile acid pendants. Biomacromolecules 18, 2663–2668. https://doi.org/10.1021/acs.biomac.7b00860.
Lee, J., Jenjob, R., Davaa, E., Yang, S.-G., 2019. NIR-responsive ROS generating core and ROS-triggered 5′-Deoxy-5-fluorocytidine releasing shell structured water-swelling microgel for locoregional combination cancer therapy. J. Contr. Release 305, 120–129. https://doi.org/10.1016/j.jconrel.2019.05.016.
Lekjinda, K., Sunintaboon, P., 2023. Green synthesis of quaternized chitosan nanogel using emulsion-photopolymerization as redox-responsive drug carrier. Carbohydr. Polym. 304, 120495. https://doi.org/10.1016/j.carbpol.2022.120495.
Liu, P., Pearce, C.M., Anastasiadi, R.-M., Resmini, M., Castilla, A.M., 2019. Covalently crosslinked nanogels: an NMR study of the effect of monomer reactivity on composition and structure. Polymers 11. https://doi.org/10.3390/polym11020353.
Longenecker, R., Mu, T., Hanna, M., Burke, N.A.D., Stöver, H.D.H., 2011. Thermally responsive 2-hydroxyethyl methacrylate polymers: soluble–insoluble and soluble–insoluble–soluble transitions. Macromolecules 44, 8962–8971. https://doi.org/10.1021/ma201528r.
Qureshi, M.A., Khatoon, F., 2019. Different types of smart nanogel for targeted delivery. J. Sci.: Advanced Materials and Devices 4, 201–212. https://doi.org/10.1016/j.jsamd.2019.04.004.
Ratanajanchai, M., Tanwilai, D., Sunintaboon, P., 2013. Visible light-induced surfactant-free emulsion polymerization using camphorquinone/tertiary amine as the initiating system for the synthesis of amine-functionalized colloidal nanoparticles. J. Colloid Interface Sci. 409, 25–31. https://doi.org/10.1016/j.jcis.2013.07.043.
Ristić, T., Hribernik, S., Fras-Zemljič, L., 2015. Electrokinetic properties of fibres functionalised by chitosan and chitosan nanoparticles. Cellulose 22, 3811–3823. https://doi.org/10.1007/s10570-015-0760-6.
Sahni, J.K., Chopra, S., Ahmad, F.J., Khar, R.K., 2008. Potential prospects of chitosan derivative trimethyl chitosan chloride (TMC) as a polymeric absorption enhancer: synthesis, characterization and applications. J. Pharm. Pharmacol. 60, 1111–1119. https://doi.org/10.1211/jpp.60.9.0001.
Seuring, J., Agarwal, S., 2013. Polymers with upper critical solution temperature in aqueous solution: unexpected properties from known building blocks. ACS Macro Lett. 2, 597–600. https://doi.org/10.1021/mz400227y.
Szabová, J., Mravec, F., Mokhtari, M., Le Borgne, R., Kalina, M., Berret, J.-F., 2023. N,N,N-Trimethyl chitosan as a permeation enhancer for inhalation drug delivery: interaction with a model pulmonary surfactant. Int. J. Biol. Macromol. 239, 124235. https://doi.org/10.1016/j.ijbiomac.2023.124235.
Thanou, M., Verhoef, J.C., Junginger, H.E., 2001. Chitosan and its derivatives as intestinal absorption enhancers. Adv. Drug Deliv. Rev. 50, S91–S101. https://doi.org/10.1016/S0169-409X(01)00180-6.
Tong, G., Fang, Z., Huang, G., Jing, Y., Dai, S., Jiang, Q., Zhang, C., Feng, S.-T., Li, Z.-P., 2016. Gadolinium/DOTA functionalized poly(ethylene glycol)-block-poly (acrylamide-co-acrylonitrile) micelles with synergistically enhanced cellular uptake for cancer theranostics. RSC Adv. 6, 50534–50542. https://doi.org/10.1039/C6RA04038A.
Tran, T.N., Piogé, S., Fontaine, L., Pascual, S., 2020. Hydrogen-bonding UCST-thermosensitive nanogels by direct photo-RAFT polymerization-induced self-assembly in aqueous dispersion. Macromol. Rapid Commun. 41, 2000203. https://doi.org/10.1002/marc.202000203.
Wang, Z.H., Wang, Z.Y., Sun, C.S., Wang, C.Y., Jiang, T.Y., Wang, S.L., 2010. Trimethylated chitosan-conjugated PLGA nanoparticles for the delivery of drugs to the brain. Biomaterials 31, 908–915. https://doi.org/10.1016/j.biomaterials.2009.09.104.
Xu, L., Wang, X., Liu, Y., Yang, G., Falconer, R.J., Zhao, C.-X., 2022. Lipid nanoparticles for drug delivery. Adv Nanobiomed Res 2, 2100109. https://doi.org/10.1002/anbr.202100109.
Xu, Z., Liu, W., 2018. Poly(N-acryloyl glycinamide): a fascinating polymer that exhibits a range of properties from UCST to high-strength hydrogels. Chem. Commun. 54, 10540–10553. https://doi.org/10.1039/C8CC04614J.
Yang, D., Viitasuo, M., Pooch, F., Tenhu, H., Hietala, S., 2018. Poly(N-acryloylglycinamide) microgels as nanocatalyst platform. Polym. Chem. 9, 517–524. https://doi.org/10.1039/C7PY01950E.
Zhu, S., Wen, L., Xiao, Y., Lang, M., 2020. Poly(ε-caprolactone) with pH and UCST responsiveness as a 5-fluorouracil carrier. Polym. Chem. 11, 5173–5180. https://doi.org/10.1039/D0PY00865F.
Zhu, Y., Lowe, A.B., Roth, P.J., 2014. Postpolymerization synthesis of (bis)amide (co)polymers: thermoresponsive behavior and self-association. Polymer (Guildf) 55, 4425–4431. https://doi.org/10.1016/j.polymer.2014.07.003.